JOURNAL OF GUIDANCE, CONTROL, AND DYNAMICS
Vol. 33, No. 6, November–December 2010

Command Generation for Flexible Systems by Input Shaping and Command Smoothing

William Singhose*
Georgia Institute of Technology, Atlanta, Georgia 30332
R. Eloundou†
Schlumberger, 92142 Clambart, France
and
Jason Lawrence‡
Georgia Institute of Technology, Atlanta, Georgia 30332

DOI: 10.2514/1.50270

Aggressive motions are often discouraged when a system has flexible dynamics. Common practice suggests that smooth commands, such as S-curves, should be used to drive the system. However, smooth commands cannot be implemented on some actuators, such as the on/off thrusters used on spacecraft or on/off valves used with hydraulics and pneumatics. Furthermore, smooth commands can lead to sluggish response. A rigorous comparison of smooth and nonsmooth reference commands is presented in this paper. The evaluation is performed by treating smooth command profiles as input-shaped functions. Input shaping is a method of reducing residual vibration by convolving a sequence of impulses with a baseline reference command. By interpreting smooth commands as input-shaped functions, a common criterion for comparing smooth and nonsmooth commands is developed. The results of this comprehensive comparison indicate that input-shaped step functions are usually more efficient for reducing vibration than commonly used smooth commands. A portable tower crane is used to experimentally verify the comparison between input-shaped and smooth commands.

I. Introduction

FLEXIBLE systems are often driven by smooth command profiles such as S-curves, trigonometric transition functions, Gaussians, and cam polynomials. Common practice suggests that these reference profiles do not produce rapid motions, which induce deflection and vibration. Consequently, these commands are designed to have smooth transitions between boundary conditions. However, these methods usually fail to fully exploit the known dynamic properties of the system. Instead, they simply provide a low-pass filtering effect. While low-pass filtering can reduce residual vibration, it is inefficient because it incurs a large rise-time penalty [1,2]. Furthermore, smooth commands cannot be implemented on some actuators, such as on/off thrusters [3,4].

Rather than relying on slow-acting smooth commands to move a system, input shaping reduces vibration by convolving a baseline reference command with a sequence of impulses (an input shaper). This input-shaping process is illustrated in Fig. 1 with a step input $p(t)$ and an input shaper containing two positive impulses. The result of the convolution is a two-step command, $u(t)$. The command-shaping process shown in Fig. 1 was first proposed in the late 1950s as a means to reduce vibration in flexible systems [5,6]. It has since been implemented on a wide variety of machines [7]. For example, the performance characteristics of satellites [8–17] have been significantly improved with input shaping.

If the input-shaper impulses are chosen appropriately, then the commands generated by the input-shaping process can be compatible with on/off thruster jets [12–15,18,19]. Such a case is shown in Fig. 2. Input-shaped commands are not, in general, smooth functions. However, they can be smooth if the initial command is smooth. Such a case is shown in Fig. 3.

The key to designing an input shaper is knowledge of the system's natural frequency ω and damping ratio ζ. This information gives the amplitudes and time spacings of the impulses in the input shaper. For example, the time locations and amplitudes of the impulses shown in Fig. 1 are [5,20]

$$\begin{bmatrix} t_i \\ A_i \end{bmatrix} = \begin{bmatrix} 0 & 0.5T_d \\ \frac{1}{1+K} & \frac{K}{1+K} \end{bmatrix}, \qquad i = 1, 2 \tag{1}$$

where

$$K = e^{\left(\frac{-\zeta\omega}{\sqrt{1-\zeta^2}}\right)} \tag{2}$$

and T_d is the damped period of vibration. The input shaper given in Eq. (1) eliminates the vibration at the frequency ω. To eliminate multiple vibration modes, additional shapers or more complex shapers are required [21–24]. The design of these shapers will be addressed in Sec. III.

Significant distinctions can be made between input-shaped commands and smooth commands on the basis of their shape, design approach, and system response. In most cases, the smooth profiles have the effect of a low-pass filter, while input shaping is similar to a notch filter superimposed on whatever effect the baseline reference command produces. A few previous papers have indicated that input-shaped commands move systems faster than smooth commands [25,26]. Some work has sought to optimize the shape of S-curves and other smooth commands in order to improve their vibration suppressing qualities for specific vibration modes [27–33].

An important contribution of this paper is a procedure, which demonstrates that both smooth and input-shaped commands can be analyzed in the same way. The basic hypothesis is that smooth commands can be decomposed into a baseline function convolved with an input shaper. This analysis method is discussed in Sec. II. The technique is used to explain vibration-reducing properties of several types of smooth and input-shaped step commands. Section III then compares the rise times achieved with smooth commands to those achieved with input-shaped step commands. Section IV investigates

Received 9 April 2010; revision received 2 July 2010; accepted for publication 6 July 2010.

*Associate Professor, Woodruff School of Mechanical Engineering.
†Mechanical Engineer.
‡Research Assistant, Woodruff School of Mechanical Engineering.

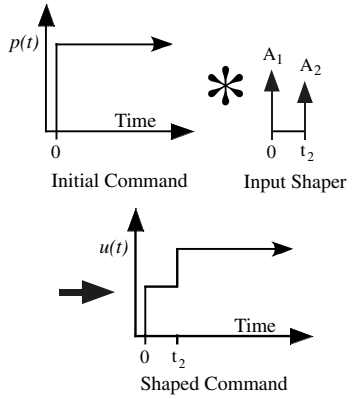

Fig. 1 Input shaping a step command.

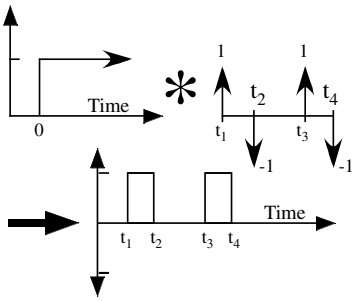

Fig. 2 Input shaping to generate on/off commands.

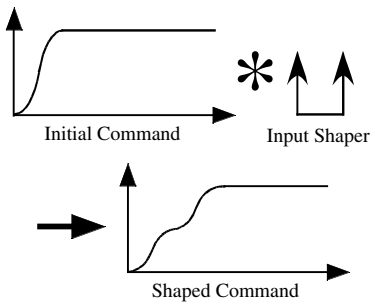

Fig. 3 Input shaping an S-curve.

robustness to modeling errors. Experimental results from a tower crane that illustrate the key findings are reported in Sec. V.

The most significant contribution of this paper is a comprehensive comparison of input shaping and command smoothing. The results of this comparison indicate that input-shaped step functions are almost always preferable to smooth commands. The only exception is when the system has a large range of uncertain modes that are much higher in frequency than the dominant low modes. Furthermore, these modes must contribute a measurable amount of amplitude to the residual vibration response for command smoothing to be needed. In this special case, a very aggressive smooth command can replace the baseline step command in the input-shaping process. Therefore, there are special situations when an intelligent combination of command smoothing and input shaping is a judicious and effective solution.

II. Decomposition of Smooth Commands

To identify the baseline function and the corresponding input shaper that produces a smooth command, it is useful to convert the command $r(t)$ from the time domain into the Laplace domain. Thus, the Laplace transform of the command, $R(s)$, is the product of the baseline function $B(s)$ with a sequence of impulses $I(s)$:

$$R(s) = B(s)I(s) = B(s)\sum_{i=1}^{n} A_i e^{-t_i s} \tag{3}$$

where n is the number of impulses, and A_i and t_i are the amplitudes and time locations of the impulses, respectively. This deconvolution is always possible for any command $R(s)$. For example, a fundamental case that always works is when a single unity-magnitude impulse is used as the impulse sequence. This results in the trivial answer of $B(s) = R(s)$. The challenge is to deconvolve meaningful input shapers that indicate what vibration frequencies the smooth command will eliminate.

A. Position S-Curves (Triangular and Trapezoidal Velocities)

As an illustration, consider an S-curve in displacement with a unit rise. This position profile is a piecewise function described by

$$r(t) = \begin{Bmatrix} 2\left(\frac{t}{R_c}\right)^2 & 0 \le t < \frac{R_c}{2} \\ -2\left(\frac{t}{R_c}\right)^2 + 4\left(\frac{t}{R_c}\right) - 1 & \frac{R_c}{2} \le t < R_c \\ 1 & R_c \le t \end{Bmatrix} \tag{4}$$

where R_c is the rise time of the S-curve. Taking the Laplace transform of $r(t)$, one obtains

$$R(s) = \frac{4}{R_c^2 s^3}\left(1 - 2e^{\frac{-R_c}{2}s} + e^{-R_c s}\right) \tag{5}$$

Expression (5) is the product of two functions:

$$B(s) = \frac{4}{R_c^2 s^3} \tag{6}$$

and

$$I(s) = 1 - 2e^{\frac{-R_c}{2}s} + e^{-R_c s} \tag{7}$$

In the time domain, this product represents the convolution of the baseline function

$$b(t) = 2\left(\frac{t}{R_c}\right)^2, \qquad t \ge 0 \tag{8}$$

with a sequence of impulses given by

$$i(t) = 1 - 2\delta\left(t - \frac{R_c}{2}\right) + \delta(t - R_c) \tag{9}$$

Figure 4 shows this convolution for the case of $R_c = 1$ s. It is now obvious than an S-curve can be considered as an input-shaped command, where the baseline function is given in Eq. (8) and the input shaper is given in Eq. (9) or, more explicitly, as

$$\begin{bmatrix} t_i \\ A_i \end{bmatrix} = \begin{bmatrix} 0 & \frac{R_c}{2} & R_c \\ 1 & -2 & 1 \end{bmatrix}, \qquad i = 1, 2, 3 \tag{10}$$

If the S-curve has a constant-velocity center section, then the convolution process would be as shown in Fig. 5. If the S-curve in Fig. 5 is a displacement function, then it corresponds to a trapezoidal velocity profile with a maximum velocity v_m and an acceleration of α. (The S-curve in Fig. 4 corresponds to a triangular velocity profile.) In this case, the baseline function is similar to the one in Eq. (8),

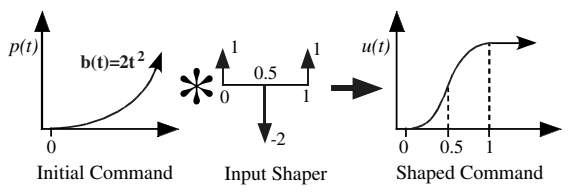

Fig. 4 Convolution to produce a position S-curve (triangular velocity).

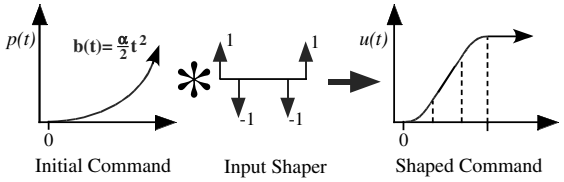

Fig. 5 Convolution to produce an S-curve with a constant-velocity segment (trapezoidal velocity).

$$b(t) = \left(\frac{\alpha}{2}\right)t^2, \qquad t \geq 0 \tag{11}$$

and the shaper is given by

$$\begin{bmatrix} t_i \\ A_i \end{bmatrix} = \begin{bmatrix} 0 & \frac{v_m}{\alpha} & \frac{x_d}{v_m} & \frac{v_m}{\alpha} + \frac{x_d}{v_m} \\ 1 & -1 & -1 & 1 \end{bmatrix}, \qquad i = 1, \ldots, 4 \tag{12}$$

where x_d is the desired displacement.

B. Residual Vibration Analysis

Decomposing a command into an input shaper and a baseline function offers benefits for residual vibration analysis. If the input shaper causes no residual vibration when applied to the system, then the shaped input (the smooth function) will also cause no residual vibration. A special exception arises when the baseline function continually drives the system in a periodic manner. This special case will be discussed in Sec. II.D.

Figure 6 shows the magnitudes of the Fourier transforms of $b(t)$, $i(t)$, and $r(t)$ for the S-curve shown in Fig. 4. When viewed in the Fourier domain, it is clear that the baseline function is a low-pass filter. On the other hand, the input shaper is a multinotch filter. For this particular example, it eliminates frequencies at 2, 4, 6 Hz, etc. The transform of the S-curve is obtained by multiplying the transform of the baseline function and the transform of the input shaper. Therefore, the S-curve is a combination of low-pass and multinotch filters. Using this Fourier description, it is easy to predict some properties of an S-curve command. For example, it is clear that the command cannot excite systems that have modes corresponding to the notch frequencies at 2, 4, 6 Hz, etc. It is also apparent that high frequencies will not be excited by the S-curve.

As an example, Fig. 7 shows the percentage overshoot of an undamped second-order system that is driven by the S-curve in Fig. 4, as a function of the oscillation frequency. As expected from Fig. 6, the notch frequencies of the shaper correspond to the zero-vibration frequencies of the system response, which occur at multiples of 2 Hz for the case shown. Furthermore, if the system frequency is above 6 Hz, then there is essentially no overshoot.

The trapezoidal velocity commands generated with Eq. (12), will cause vibration responses similar to the triangular velocity profiles

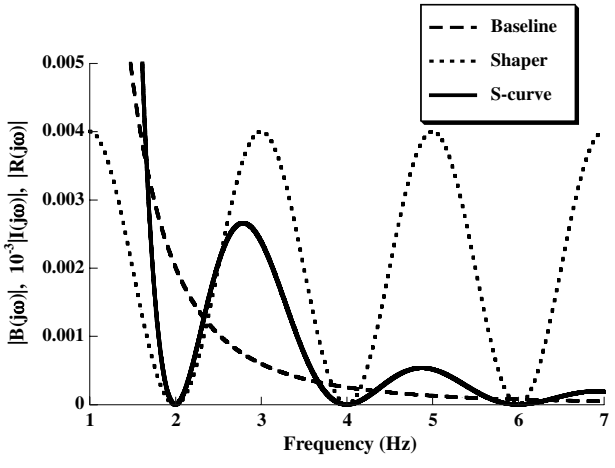

Fig. 6 Magnitudes of Fourier transforms of $r(t)$, $b(t)$, and $i(t)$.

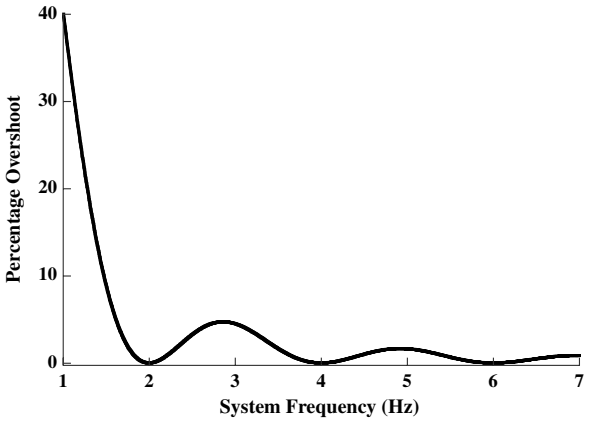

Fig. 7 Percentage overshoot of a second-order response to an S-curve.

generated with Eq. (10). However, the amplitude of vibration is a complex function of both the move distance and the velocity limit. For example, Fig. 8 shows the response of a mass-spring-mass system when the move distance is fixed at 10 units, but the velocity limit v_m is varied between 0.5 and 1.0 units/s. The spring constant was set to 1 and each of the mass values was set equal to 0.5. As the velocity limit increases, the system moves faster, but the amount of transient deflection and residual vibration changes in a complicated manner. Both the fastest and slowest commands cause approximately the same amplitude of vibration, while the intermediate velocity of 0.8 induces almost no residual vibration.

To better understand the vibration phenomenon, Fig. 9 plots the residual vibration amplitude as a function of the velocity limit. Note that when the maximum allowable velocity reaches a critical level (just over 3 units/s in this case), the coast period goes away and the trapezoidal velocity command converges to a triangular velocity (S-curve in position) command. After this point, increasing the maximum allowable velocity has no effect on the command. Figure 10 shows the residual vibration amplitude as a function of both the move distance and the maximum velocity over a fairly small region of parameter values. Even over this small area, the amplitude of vibration varies widely and is a complicated function of the two motion parameters.

Plots of the magnitude of the Fourier transform of the command signals, such as those in Fig. 6, offer immediate insight into the vibratory response of a system driven by the command [34]. However, they are not the most useful representation for describing input-shaper effectiveness. The weakness lies in the nonintuitive units on the vertical axis. When the magnitude of the Fourier transform is nonzero, it is unclear if the vibration is large or small.

Input shapers are usually assessed using a *sensitivity curve* that has a percentage residual vibration on the vertical axis. This representation shows how much vibration occurs with input shaping compared to the vibration without input shaping. Note that this

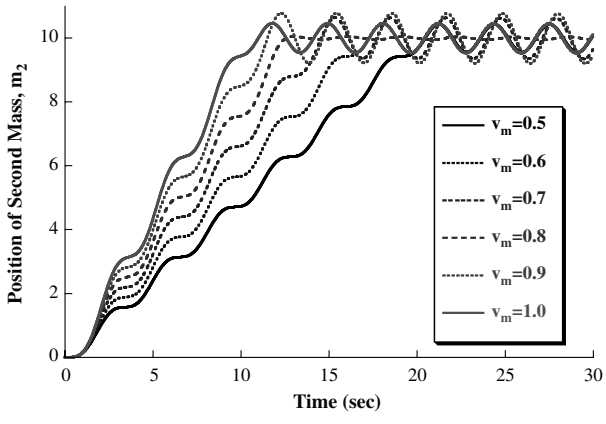

Fig. 8 Mass-spring-mass response to trapezoidal velocity commands.

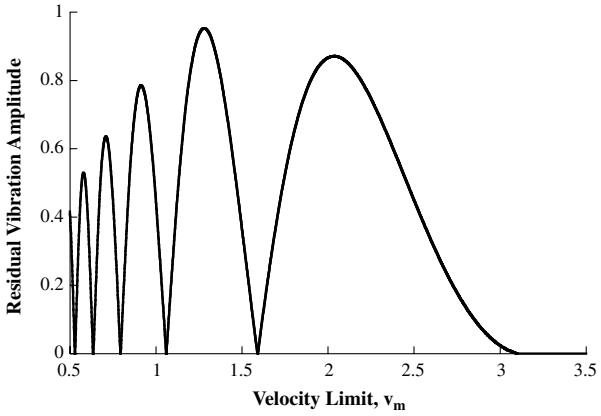

Fig. 9 Residual vibration amplitude vs velocity limit of trapezoidal velocity commands.

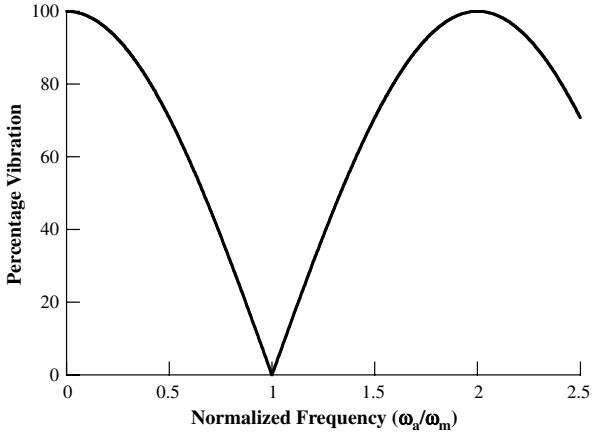

Fig. 11 Sensitivity curve for a ZV shaper.

representation is more similar to the percentage overshoot shown in Fig. 7 than the Fourier magnitude shown in Fig. 6. Furthermore, the horizontal axis of a sensitivity curve is often labeled with a normalized frequency formed by dividing the actual natural frequency, ω_a, by the modeled natural frequency, ω_m.

Figure 11 shows the sensitivity curve for the zero-vibration (ZV) shaper given in Eq. (1). The shaper will cause no vibration when the modeling frequency is correct ($\omega_a/\omega_m = 1$). However, if there is a modeling error, then there can be a considerable amount of residual vibration. If the model is off by a factor of 2, then the ZV shaper will induce the same amount of vibration as when input shaping is not used. This is the worst possible case, because the sensitivity curve for the ZV shaper never exceeds 100%.

Given that S-curves can be decomposed into a baseline function convolved with an input shaper and input-shaper effectiveness can be measured using sensitivity curves, S-curves and input-shaped step commands can now be directly compared. A very important result of this decomposition analysis is that the shaper in Eq. (10) used to construct the S-curve has a duration that is twice the period of the first vibration mode that it suppresses. (In the above example, the S-curve had a duration of 1 s and the first mode it cancelled was 2 Hz.) The S-curve input-shaper duration is very long compared to traditional input shapers. The duration of the ZV shaper given in Eq. (1) is only one-half of the period of the vibration. Note that the second impulse in the S-curve shaper has a negative amplitude. If an input shaper is allowed to contain a negative impulse, then it can suppress vibration even faster. For example, the unity-magnitude ZV (UMZV) shaper given by

$$\begin{bmatrix} t_i \\ A_i \end{bmatrix} = \begin{bmatrix} 0 & \frac{T_d}{6} & \frac{T_d}{3} \\ 1 & -1 & 1 \end{bmatrix}, \qquad i = 1, 2, 3 \tag{13}$$

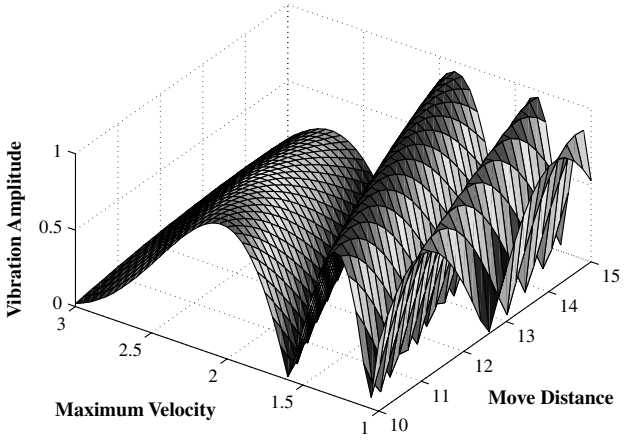

Fig. 10 Vibration induced by a trapezoidal velocity command.

is only one-third of a vibration period [35]. Therefore, in order to cancel vibration, an S-curve must be four times longer than a command formed by shaping a step function with a ZV shaper, or six times longer than a command formed with a UMZV shaper. This time lag of the S-curve translates into sluggish system response. The benefit of the S-curve is a low-pass filtering effect that is entirely unneeded unless the system has problematic high frequencies. Comparisons of command effectiveness on multimode systems will be discussed in Sec. III.

C. Other Smooth Commands

The deconvolution analysis presented above is not limited to S-curves. It can be applied to other types of smooth command profiles, such as versine functions and transition profiles resulting from the superimposition of ramps and sinusoidal functions. Consider a smooth trigonometric transition function with a single change in concavity during the rise:

$$r_2(t) = \begin{Bmatrix} \frac{t}{R_t} - \frac{1}{2\pi}\sin\left(\frac{2\pi}{R_t}t\right), & 0 \le t < R_t \\ 1 & R_t \le t \end{Bmatrix} \tag{14}$$

where R_t is defined to be the rise time of the transition function. In the Laplace domain, Eq. (14) corresponds to

$$R_2(s) = \frac{4\pi^2}{R_t s^2(R_t^2 s^2 + 4\pi^2)}(1 - e^{-R_t s}) \tag{15}$$

Therefore, the baseline command is given by

$$b_2(t) = \frac{t}{R_t} - \frac{1}{2\pi}\sin\left(\frac{2\pi}{R_t}t\right) \tag{16}$$

The input shaper associated with the above baseline command is

$$\begin{bmatrix} t_i \\ A_i \end{bmatrix} = \begin{bmatrix} 0 & R_t \\ 1 & -1 \end{bmatrix}, \qquad i = 1, 2 \tag{17}$$

D. Periodic Baseline Functions

When the deconvolution analysis yields a periodic baseline function, as was the case for the transition function above, the system may respond in an oscillatory manner at the period of the baseline function. This oscillation can occur even when the input-shaper analysis predicts zero residual vibration. This does not mean that the analysis is faulty. Rather, it means that the command has a component function that is driving the system in a periodic manner, so the system will naturally have some response to the periodic portion of the command.

Consider another case where the smooth command is a piecewise versine reference command of rise time R_v defined as

$$r_3(t) = \begin{Bmatrix} \text{vers}\left(\frac{2\pi}{3R_v}t\right), & 0 \le t < \frac{R_v}{2} \\ \text{vers}\left(\frac{2\pi}{3R_v}t\right) - \text{vers}\left(\frac{2\pi}{3R_v}\left(t - \frac{R_v}{2}\right)\right), & \frac{R_v}{2} \le t < R_v \\ 1 & R_v \le t \end{Bmatrix} \quad (18)$$

where

$$\text{vers}\,(\cdots) = 1 - \cos(\cdots) \quad (19)$$

Converting Eq. (18) into the Laplace domain yields

$$R_3(s) = \frac{4\pi^2}{s(9R_v^2 s^2 + 4\pi^2)}\left(1 - e^{\frac{-R_v}{2}s} + e^{-R_v s}\right) \quad (20)$$

The corresponding time-domain function $r_3(t)$ is composed of the baseline function

$$b_3(t) = \text{vers}\left(\frac{2\pi}{3R_v}t\right) \quad (21)$$

and the input shaper:

$$\begin{bmatrix} t_i \\ A_i \end{bmatrix} = \begin{bmatrix} 0 & \frac{R_v}{2} & R_v \\ 1 & -1 & 1 \end{bmatrix}, \qquad i = 1, 2, 3 \quad (22)$$

The input shaper in Eq. (22) is equivalent to the UMZV shaper in Eq. (13) when R_v is set equal to one-third of the system oscillation period. A sensitivity curve for the UMZV shaper is shown in Fig. 12. Of course, the residual vibration at the modeling frequency ($\omega_a/\omega_m = 1$) is zero. But note that the sensitivity curve reaches a maximum of 300% at several high frequencies. In other words, those modes will be excited three times more than without input shaping. However, given that the shaper in Eq. (22) is used in conjunction with the low-pass filtering effect of the baseline function in Eq. (21), it is unlikely that high-mode excitation will be a problem.

Given the equivalence between the versine shaper in Eq. (22) and the UMZV shaper in Eq. (13), it would seem that vibration could be eliminated by setting R_v equal to one-third the system period. For example, R_v would be set to 1/3 s to suppress a 1 Hz frequency. Figure 13 shows the percentage overshoot of an undamped second-order system driven by such a versine function, as a function of the system frequency. Perhaps unexpectedly, the vibration of a 1 Hz system is not suppressed, as was predicted by the sensitivity curve in Fig. 12. Note, however, that the higher sensitivity curve zeros at 5, 7, 11 Hz, etc., are zero overshoot frequencies in Fig. 13.

The explanation lies in the baseline function and how it affects the pole/zero cancellation provided by the input shaper. Since the earliest descriptions of input shaping in the 1950s, it has been known that input shaping creates commands that have zeros near the flexible poles of the system [6,34,36,37]. In the case of an undamped second-order system, the plant transfer function has two purely complex

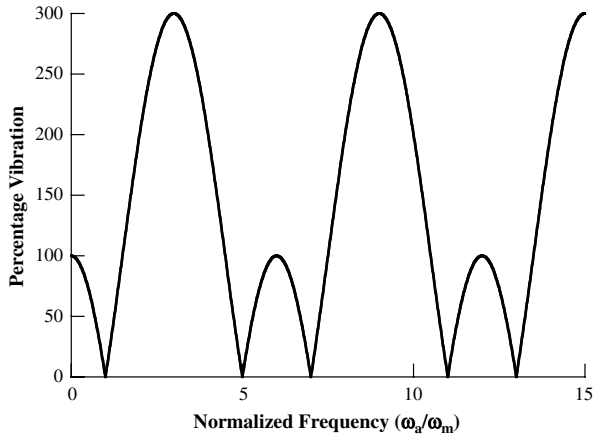

Fig. 12 Sensitivity curve for UMZV input shaper.

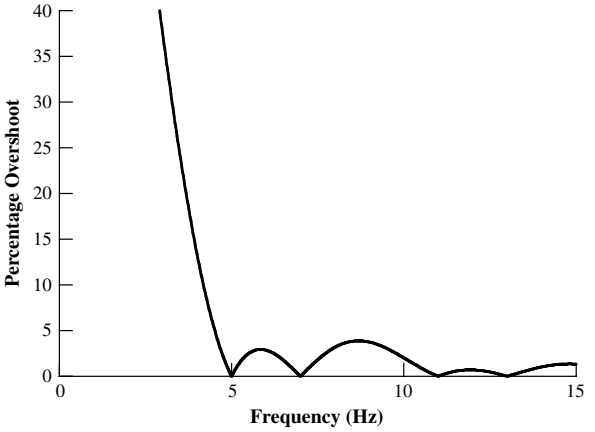

Fig. 13 Percentage overshoot in response to versine function.

poles located at the system natural frequency, ω_n. The UMZV shaper places zeros along the imaginary axis, as shown explicitly in Fig. 14a and also by the notch frequencies in Fig. 12. The zeros are located at k multiples of the modeling frequency, where $k = 1, 5, 7, 11, \ldots$. The first pair of zeros overlay the system's vibratory poles.

A special case arises when the baseline command is a trigonometric function that has its own poles, such as the versine function in Eq. (21). To examine this effect, consider the case above where $R_v = 1/3$ s. For a 1 Hz (2π rad/s) vibration, which should be eliminated by the UMZV shaper, the vibration period is $2\pi/\omega_n$, so

$$R_v = \frac{2\pi}{3\omega_n} \quad (23)$$

Now substitute Eq. (23) into the Fourier transform of $b_3(t)$ to get

$$B_3(j\omega) = \frac{1}{j\omega\left(\frac{(j\omega)^2}{\omega_n^2} + 1\right)} \quad (24)$$

The above expression shows that the baseline command of the versine profile, $b_3(t)$, adds an additional pair of purely complex poles located at $\omega = \omega_n$. These coincide with the poles from the flexible system, as shown in Fig. 14b. The UMZV shaper can cancel only one of the poles at $\omega = \omega_n$. Therefore, to achieve zero vibration in the shortest possible time, the second pair of zeros from the UMZV shaper must be used to cancel the flexible poles of the system. (The first pair of zeros provided by the UMZV shaper must cancel the complex poles of the versine function.) To accomplish this cancellation, the rise time of the versine function must be increased by a factor of 5. The resulting pole/zero cancellation is illustrated in Fig. 14c.

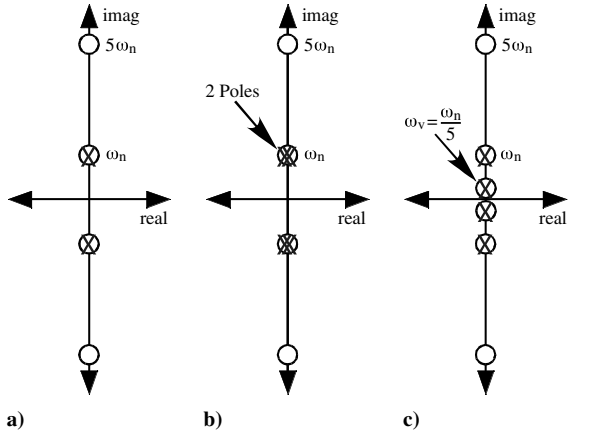

Fig. 14 Pole/zero cancellation effects: a) UMZV shaper, b) versine function plus UMZV shaper, and c) slowed versine plus UMZV shaper.

To summarize, the fastest rise time to suppress vibration using a versine profile is

$$R_v = \frac{10\pi}{3\omega_n} = \frac{5T}{3} \tag{25}$$

This is five times slower than a step input convolved with a UMZV shaper. However, it is slightly faster than the S-curve command, which requires a rise time of $2T$ to cancel a vibrational mode.

This example illustrates that one can gain valuable insight from analyzing the input-shaper component of a smooth profile. However, care must be taken if the baseline function that arises from the analysis is periodic. The periodic function will provide additional poles that drive the system in a periodic manner.

III. Rise-Time Comparison

The previous section showed that canceling vibration by using smooth commands takes much longer than with input-shaped step commands. This section more thoroughly compares the rise times of input-shaped step commands and smooth commands by examining a range of systems.

A. Single-Mode Systems

In this subsection, smooth commands and input-shaped steps are used to drive a second-order harmonic oscillator characterized by

$$G(s) = \frac{\omega_n^2}{s^2 + 2\zeta\omega_n s + \omega_n^2} \tag{26}$$

Figure 15 shows the residual vibration induced by several S-curves, as a function of the system frequency when $\zeta = 0$. The residual vibration is measured by the percentage overshoot. Each line corresponds to a different S-curve rise time R_c. The curves are shifted in frequency and their widths are stretched by a factor inversely proportional to R_c. Specifically, the rise time of the S-curve is related to its first notch frequency f_1 by

$$f_1 = \frac{2}{R_c} \tag{27}$$

This is the lowest vibration frequency that can be suppressed with an S-curve command. Stated differently, to suppress a vibration frequency, the rise time of the S-curve must be twice the period of the vibration being suppressed.

For comparison purposes, a step command convolved with a ZV shaper is applied to the same system. The shaping process increases the rise time of the baseline command by the duration of the shaper. The rise time of the ZV shaper, R_{ZV}, is equal to one-half of the vibration period:

$$R_{ZV} = 0.5T_1 \tag{28}$$

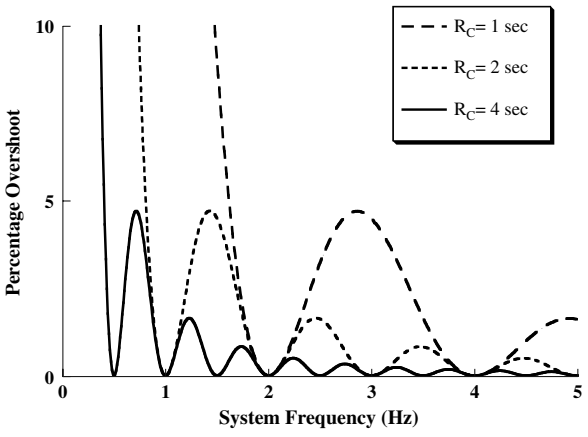

Fig. 15 Effects of S-curve rise time on residual vibration of a second-order system.

Combining Eqs. (27) and (28) yields

$$R_{ZV} = 0.25R_c \tag{29}$$

Therefore, eliminating vibration with an S-curve takes four times longer than when using a step command shaped with a ZV shaper.

The relationship in Eq. (29) applies strictly to the rise times of the *commands*. The rise times of the system *response* that the commands induce are somewhat different. However, the rise time of the system will approximately track the rise time of the command. This is shown in Fig. 16, where the 99% rise time of a second-order system is plotted versus the natural frequency of the system for different R_c values. The response rise time varies somewhat, but it is close to the rise time of each of the 3 S-curves shown. The frequencies cancelled by each S-curve are denoted by X. These frequencies are the troughs shown in Fig. 15.

For comparison, Fig. 16 also includes the rise time when a ZV-shaped step input is used. Comparing the rise time of the shaped step to the first frequency canceled by the S-curves (the first X on each curve) reveals that the shaped step produces a rise time that is approximately four times faster in each case. This confirms Eq. (29) as a valid rise-time measurement.

Referring back to Fig. 15, it is obvious that the S-curves only cancel select frequencies. However, the ZV-shaped step commands cancel vibration at every frequency shown in Fig. 16. This exact cancellation occurs because a different ZV shaper is used for each of the frequencies shown in the figure. On the other hand, the S-curves are not designed to suppress each individual frequency. Rather, they are designed by setting their rise time to achieve a desired roll-off frequency.

The time savings provided by the ZV shaper should not be surprising. Input shaping uses knowledge of the natural frequency and damping ratio to directly target the vibration problem. On the other hand, the S-curve profile relies on its smoothness to minimize the excitation of all vibrations above its roll-off frequency. Furthermore, the input-shaper impulse time locations and amplitudes constitute control parameters that can be varied. When using an S-curve, only the command rise time can be adjusted to affect the vibration suppression.

B. Two-Mode Systems

Consider an undamped two-mode system represented by the following state-space model:

$$A = \begin{bmatrix} 0 & 1 & 0 & 0 \\ -\omega_1^2 & 0 & 0 & 0 \\ 0 & 0 & 0 & 1 \\ 0 & 0 & -\omega_2^2 & 0 \end{bmatrix} \qquad B = [0 \quad 1 \quad 0 \quad 1]^T$$

$$C = [0 \quad 1 \quad 0 \quad 1] \qquad D = 0 \tag{30}$$

Assume a specific case when the natural frequencies are 2 and 3.1 Hz. First, an S-curve reference command is used to drive the system. As noted earlier, the low-pass filtering effect of the S-curve

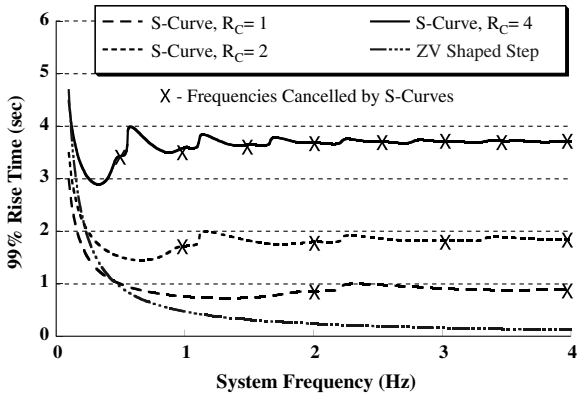

Fig. 16 Rise time of a second-order system.

profile helps reduce high-frequency vibrations. Therefore, for this case, R_c could be chosen to only ensure that the residual vibration from the 2 Hz mode is eliminated. However, this does not mean that there will be zero vibration at 3.1 Hz. This becomes evident by reexamining the dashed line in Fig. 15. If R_c is 1 s, then the vibration at 2 Hz is completely eliminated; however, there will be some amount of vibration at 3.1 Hz. Thus, a better solution might come from choosing $R_c = 2$ s, because this command eliminates 2 Hz and also suppresses frequencies near 3 Hz, as shown by the dotted line in Fig. 15.

It is evident that the design of S-curves for multimode systems is not well defined. Nevertheless, S-curves can be designed to completely cancel two vibration modes. The dashed line in Fig. 17 shows the command duration as a function of the mode ratio ω_2/ω_1 when S-curves are designed to completely suppress two undamped modes. Mode ratios that are close to integer numbers can be cancelled with an S-curve whose duration is approximately twice the low-mode period. This is because the S-curve shaper in Eq. (10) provides a multinotch filtering effect that cancels integer multiples of the low frequency. However, Fig. 17 demonstrates that the rise time can be considerably lengthened for multimode systems when S-curves are used to suppress vibration.

Input shaping is straightforward to use on multimode systems [21,23,24,38]. Shapers designed for each mode separately can simply be convolved to create a shaper that will eliminate both modes. The process can be extended to any number of modes. Instead of convolving single-mode shapers together, rise time can be improved somewhat by simultaneously solving the vibration constraints for each mode [21]. The solid line in Fig. 17 shows the rise time for a two-mode ZV shaper as a function of the mode ratio. Note that for all mode ratios it is substantially faster than an S-curve, which is shown by the dashed line. For 2 and 3.1 Hz modes, the two-mode ZV shaper obtained by direct solution is

$$\begin{bmatrix} t_i \\ A_i \end{bmatrix} = \begin{bmatrix} 0 & 0.1959 & 0.3918 \\ 0.281 & 0.438 & 0.281 \end{bmatrix}, \qquad i = 1, 2, 3 \tag{31}$$

Note that the rise time of a step convolved with the two-mode ZV shaper is only 0.4 s, as opposed to the 2 s rise time needed for a comparably effective S-curve. In this case, the S-curve is five times longer than the corresponding input-shaped step input. Therefore, for two-mode systems, the benefits of using input-shaped step inputs, as opposed to S-curve commands, can be even greater than for single-mode systems.

Given the significant rise-time advantage of input-shaped step commands, it is obvious that S-curves are a poor alternative for applications requiring rapid motion. However, S-curves have the advantage of providing a low-pass filtering effect that does not occur with shaped steps. Therefore, a reasonable approach for some special types of multimode systems is to combine input shaping and command smoothing. The smooth command should not attempt to cancel the low mode; it is too slow for that. But a smooth command could be used to attenuate the high frequencies without a significant time penalty. For the two-mode case considered in this section, the input shaper can be designed to suppress the low mode, and the first notch in the S-curve frequency response can be set at the second mode, using Eq. (27). The rise time using this shaped-smooth command is shown by the dotted line in Fig. 17. This approach is a significant improvement over just using S-curves, but it is still sluggish compared to the two-mode input-shaped step inputs.

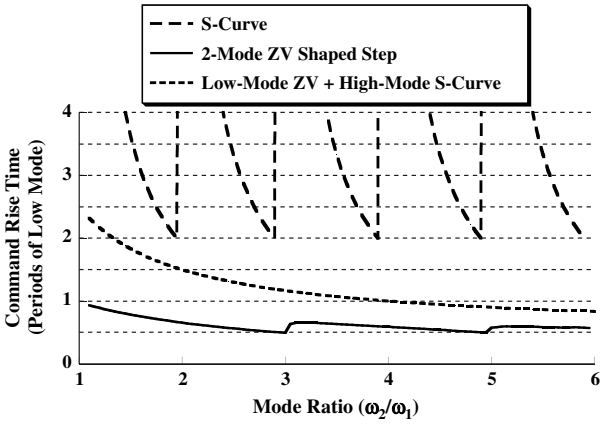

Fig. 17 Time required to eliminate vibration in two-mode systems.

C. Systems with One Low Mode and a Range of High Modes

The two previous categories of single- and double-mode systems certainly do not characterize all flexible systems. Another important class of systems has one dominant low mode and a range of high frequencies. Accordingly, in this section an example system with a 1 Hz mode and high-mode vibrations in the 20–80 Hz frequency range is investigated.

When designing an S-curve command for the above system, its rise time might be selected to be $R_c = 2$ s in order to cancel the 1 Hz mode. The high modes would then be suppressed by the low-pass filtering effect shown in Figs. 6 and 7. As the distance from the first notch frequency to the higher frequencies increases, the low-pass filtering of the S-curve becomes more effective. Hence, for systems with a low mode and higher-order modes that are sufficiently above the low mode, an effective S-curve can be designed only using the low-mode frequency. Stated differently, high frequencies can be cancelled at no extra cost in rise time. In spite of this advantage, the rise-time duration of S-curves remains a drawback compared to input shaping.

Input shaping is efficient for multimode systems and for high-mode limiting (HML) [39]. An input shaper can be designed to suppress the residual vibrations below a tolerable level, V_{tol} [24,40,41]. For the example here, V_{tol} was set to 1% and the residual vibration was suppressed between 20 and 80 Hz. The HML input shaper obtained from these design constraints was then convolved with a ZV shaper designed to suppress the 1 Hz mode. The complete shaper suppresses the vibration to zero at 1 Hz and below 1% for frequencies between 20 and 80 Hz. The rise time of a step input convolved with the ZV-HML shaper is only 0.58 s. This is over 70% faster than the corresponding 2 s S-curve that would be appropriate for this system.

On these types of systems, S-curves and HML shapers offer different advantages. Ideally, one would want a fast-rising input that cancels the low mode and suppresses the high modes. Therefore, intelligently combining the two command generation approaches, as was done for the two-mode system, can yield a good solution. A useful combination is achieved by convolving a very fast-rising S-curve with an input shaper designed to suppress only the low mode.

Figure 18 shows a conceptual representation of this combined effect. The frequency response curve shows a lightly damped low mode at 2π rad/s (1 Hz). This peak would be counteracted by a single-mode input shaper. The high frequencies starting at 20 Hz

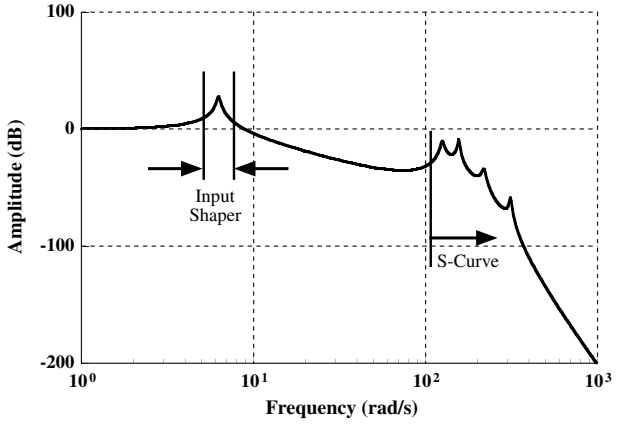

Fig. 18 Targeted frequencies by low-mode shaper combined with fast S-curve.

would be partially suppressed by the action of the low-mode shaper. However, to ensure full suppression, the roll-off frequency of the S-curve used as the baseline command is chosen to just precede the high frequencies. From Eq. (27), we know that the rise time of the S-curve is governed by the lower end of the high-mode range. Consequently, for a range of frequencies above 20 Hz, R_c should be 0.1 s. When added to the duration of the ZV shaper designed for 1 Hz, the total rise time of the ZV-shaped S-curve is only 0.6 s. Therefore, such a command has a rise time comparable to the ZV-HML shaper (0.58 s duration).

This section has demonstrated that, for single-mode or multimode systems, input-shaped step commands yield significantly shorter rise times than S-curves. However, an input-shaped step and an input-shaped aggressive S-curve are comparable in duration whenever the system exhibits a low mode and a high mode, or a range of modes that are significantly higher than the low mode. Therefore, only systems with a wide range of problematic and uncertain high modes should be driven with input-shaped S-curve commands. In the absence of such special conditions, an input-shaped step command can eliminate vibration much faster than an S-curve.

IV. Robustness to Modeling Errors

In many cases, the system frequencies may not be known accurately. It then becomes important to evaluate how this uncertainty can translate into residual vibration. In this section, three shapers are compared based upon their sensitivity to modeling errors. Two of these input shapers are the ZV shaper given in Eq. (1), and the S-curve (SC) shaper given in Eq. (10). The third input shaper evaluated is the extra-insensitive (EI) shaper [42], which is much more robust than the ZV shaper, but lengthens the rise time.

The sensitivity curves of the three different shapers are shown in Fig. 19. The insensitivity, defined as the width of each curve that lies below a specified vibration level, provides a quantitative measure of robustness. The ZV and SC shapers have a comparable 5% insensitivity (the curve width at 5%). By contrast, the EI has a 5% insensitivity almost seven times more than the other two shapers. This increased robustness is accomplished with a rise time equal to twice the duration of the ZV shaper, but only half the duration of the SC shaper.

Analyzing only the shapers may not be sufficient to evaluate the entire robustness properties of a command signal. This is because the shapers may be convolved with baseline functions that have their own vibration-reducing properties. The situation considered here is when the SC shaper is convolved with the baseline function in Eq. (8) and the ZV and EI shapers are convolved with a step function. In this case, the baseline function used with the SC shaper is much less aggressive. Therefore, it will act to further decrease vibration at high frequencies. In addition, the physical hardware that is being moved will also provide some filtering effects. Therefore, an exact comparison of the robustness properties can only be performed through experimentation on the actual machine. However, the sensitivity curve for the EI shaper clearly demonstrates that large robustness to modeling errors can be attained while driving a system twice as fast as with an S-curve.

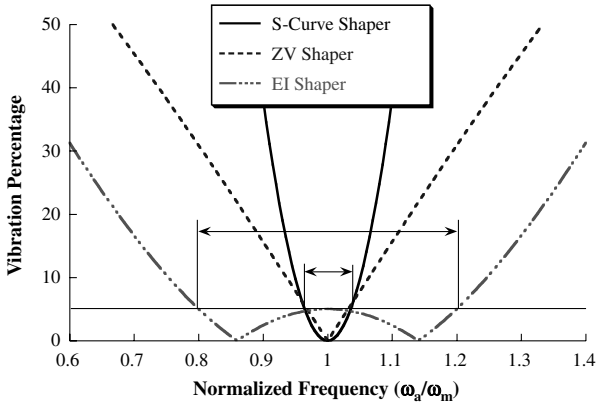

Fig. 19 Sensitivity curves for ZV, S-curve, and EI shapers.

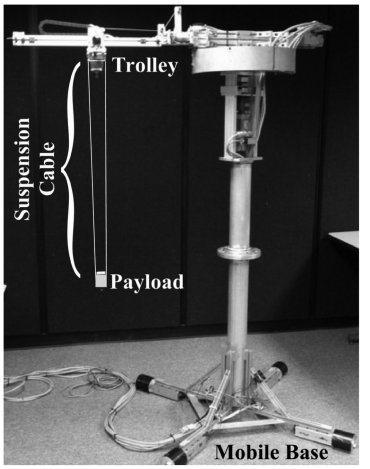

Fig. 20 Portable tower crane.

V. Experimental Results

To verify some of the key results presented here, experiments were performed on a tower crane located at the Tokyo Institute of Technology [43]. The crane, shown in Fig. 20, is approximately 2 m high, and the outer limit of its reachable work space forms a 2-m-diam circle. The crane rotates about the vertical axis; its trolley moves in and out relative to the support tower; and it hoists a payload up and down. Encoders measure the radial, angular, and hoisting motion. A downward-looking camera mounted on the trolley measures the payload swing.

Crane motion is controlled in one of three modes: 1) local manual control via a joystick and on-off buttons, 2) remote operation via the internet that uses a graphical user interface that mimics the local control box, and 3) fully automated motion where complete trajectories can be downloaded to the control computer and performed without a human operator. The experiments described here were conducted in the fully automated mode.

Several components of the crane control system can be varied. There are internal feedback gains in the motor controllers that determine how well the motors track the desired trajectories. The sampling frequency of the overhead camera affects the area over which it can scan for the payload. The control parameters that are used here are the maximum acceleration, maximum velocity, input shaper, and the baseline reference command sent to the motor driver that controls the trolley motion in the radial direction. As an example, Fig. 21 shows the trolley position when several S-curves are used to move the trolley 305 mm.

The crane trolley obviously cannot make the instantaneous jumps that correspond to a shaped step input. However, the crane motors are

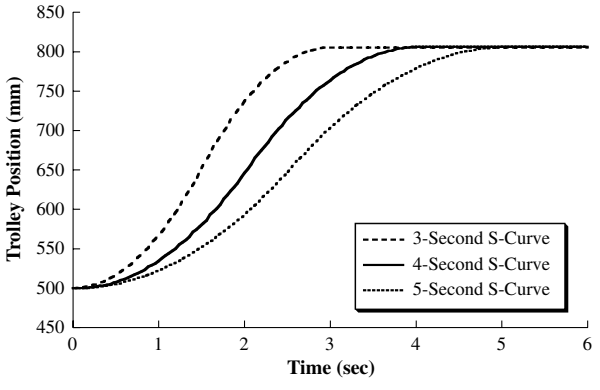

Fig. 21 Trolley response to S-curve commands.

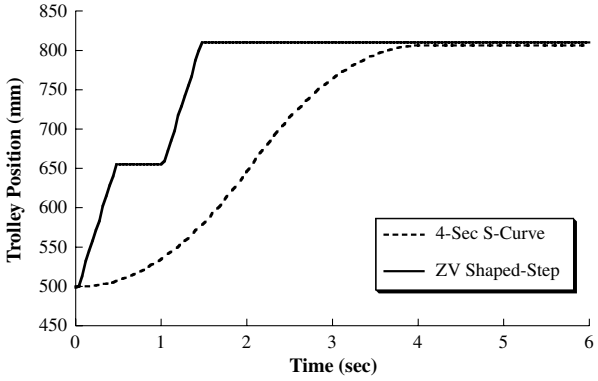

Fig. 22 Trolley response to S-curve and ZV-shaped step commands.

very powerful, so velocity and acceleration limits must be enforced to keep the hardware from being damaged by large inertia forces. The result is that the input-shaped steps are converted to steep ramp functions by the imposed actuator limits. This effect is shown in Fig. 22 for the case when the acceleration limit is 25.4 m/s^2 and the velocity limit is 0.35 m/s. The net result is that the actual rise time is approximately 1.5 s, instead of the 1 s rise requested by the input-shaped step input. (Note that the motion using a 4 s S-curve also takes slightly longer than 4 s.) This modification of the command is a common occurrence on real machines and does not pose a problem for input shaping, provided the transformation is fairly linear.

Using the well-known pendulum relationship between the payload suspension length L, the gravitational constant g, and the oscillation frequency, we know that the period of pendulum oscillation is

$$T = 2\pi\sqrt{\frac{L}{g}} \tag{32}$$

Recall that the rise time of an S-curve needs to be twice the oscillation period in order to cancel the vibration:

$$R_C = 2T = 4\pi\sqrt{\frac{L}{g}} \tag{33}$$

Solving for the pendulum length whose oscillation is canceled by an S-curve we find

$$L = g\left(\frac{R_C}{4\pi}\right)^2 \tag{34}$$

Therefore, a 4 s S-curve will cancel the oscillation of a pendulum whose length is 994 mm. Of course, the length of a crane suspension cable cannot be known with total accuracy, so it is of interest to investigate the response with various size errors in the estimation of the suspension length. The solid line in Fig. 23 shows the payload response to a 4 s S-curve when the suspension length is approximately 975 mm. As expected with such a small error, the S-curve virtually eliminates the residual vibration.

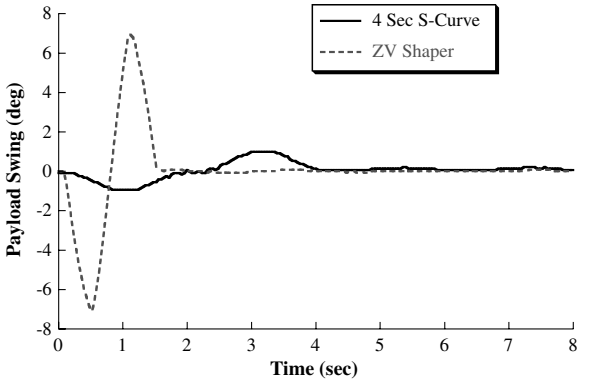

Fig. 23 Payload response with a 975 mm suspension length.

The dotted line in Fig. 23 shows the payload response resulting from a ZV-shaped step input that was designed for a 994 mm suspension length, and then subjected to the above actuator limitations. The results clearly demonstrate that the input shaping works very well. It reduces the residual payload sway to near zero. Furthermore, the 305 mm translational motion of the payload was accomplished approximately 2.6 times faster than when the S-curve was used.

When the payload is hoisted up and down, the payload oscillation frequency changes. Using the S-curve input shaper in Eq. (10), we can predict that the 4 s S-curve will cancel oscillations at 0.5, 1.0, 1.5 Hz, etc. These frequencies correspond to pendulum lengths of 994, 248, 110 mm, etc. Therefore, the 4 s S-curve would be a reasonable choice for cranes operating with a 1 m suspension length.

A series of experiments was performed using the 4 s S-curve to move payloads with various suspension lengths. The amplitude of residual vibration, as a function of the suspension length, is shown in Fig. 24. The S-curve does eliminate most of the oscillation near its primary target length of 1 m. However, as the suspension length increases, the residual vibration also increases. Furthermore, as the suspension length decreases from 1 m, the residual oscillation also increases to approximately 30 mm peak to peak. Additional decreases in the suspension length cause the vibration to decrease back towards zero as the pendulum frequency approaches the second frequency that the S-curve can cancel (1.0 Hz). Similar experiments were conducted for 3 and 5 s S-curves. The results from the entire battery of tests are shown in Fig. 25.

The experimental findings reported here confirm that the vibration analysis proposed in Sec. II can accurately predict the vibration-canceling properties of smooth commands. Furthermore, they

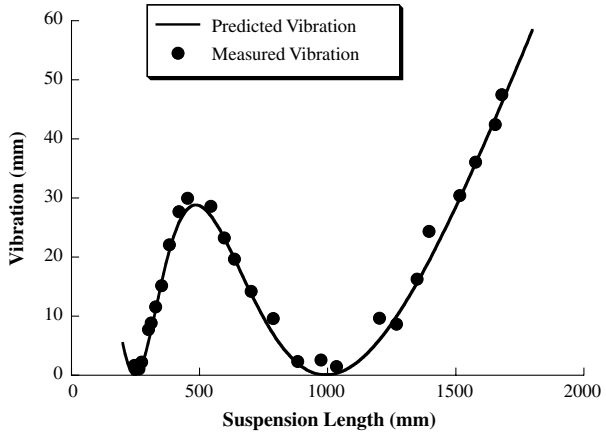

Fig. 24 Peak-to-peak residual vibration from S-curve.

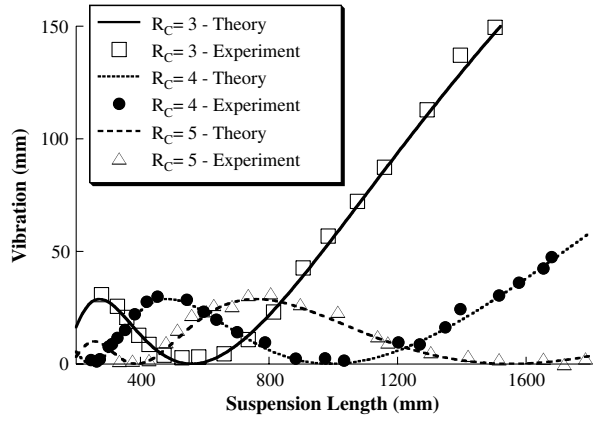

Fig. 25 Peak-to-peak residual vibration from various S-curves.

confirm the results in Sec. III, which showed that input-shaped step functions can move a system at much higher speeds than S-curves.

VI. Conclusions

Smooth reference commands can be analyzed as input-shaped functions by using a deconvolution process. This decomposition allows smooth functions to be compared with the same performance criteria as input-shaped step commands. A key result showed that S-curves must be four times slower than step commands shaped with zero-vibration shapers to eliminate vibration in a single-mode system. For multimode systems, the time savings with input-shaped steps can be even larger. When the system has an uncertain range of high-frequency modes that contribute significant vibration amplitude, a fast-rising, input-shaped S-curve can produce comparable performance to input-shaped step inputs. A robustness analysis showed input-shaped step profiles can be very robust to modeling errors, while remaining significantly faster than S-curve commands. Experimental results from a tower crane demonstrated the vibration-reducing properties of both input-shaped step and S-curve commands. Furthermore, they confirmed the large time savings of input-shaped step commands relative to S-curve commands.

Acknowledgments

The authors would like to thank Siemens Energy and Automation for providing the equipment and funding to develop the portable tower crane. Furthermore, the 21st Century Center of Excellence in Robotics at the Tokyo Institute of Technology provided additional funding and support to conduct the tower crane experiments.

References

[1] Ahmad, M. A., Ismail, R. M. T. R., Ramli, M. S., Abd Ghani, N. M., and Hambali, N., "Investigations of Feed-Forward Techniques for Anti-Sway Control of 3-D Gantry Crane System," *IEEE Symposium on Industrial Electronics and Applications*, Inst. of Electrical and Electronics Engineers, Piscataway, NJ, 2009, pp. 265–270.

[2] Singer, N., Singhose, W., and Seering, W., "Comparison of Filtering Methods for Reducing Residual Vibration," *European Journal of Control*, Vol. 5, 1999, pp. 208–218.

[3] Ben-Asher, J., Burns, J. A., and Cliff, E. M., "Time-Optimal Slewing of Flexible Spacecraft," *Journal of Guidance, Control, and Dynamics*, Vol. 15, 1992, pp. 360–67.

[4] VanderVelde, W., and He, J., "Design of Space Structure Control Systems Using On-Off Thrusters," *Journal of Guidance, Control, and Dynamics*, Vol. 6, No. 1, 1983, pp. 53–60. doi:10.2514/3.19802

[5] Smith, O. J. M., "Posicast Control of Damped Oscillatory Systems," *Proceedings of the IRE*, Vol. 45, Sept. 1957, pp. 1249–1255. doi:10.1109/JRPROC.1957.278530

[6] Smith, O. J. M., *Feedback Control Systems*, McGraw–Hill, New York, 1958, pp. 331–345.

[7] Singhose, W., "Command Shaping for Flexible Systems: A Review of the First 50 Years," *International Journal of Precision Engineering and Manufacturing*, Vol. 10, No. 4, 2009, pp. 153–168. doi:10.1007/s12541-009-0084-2

[8] Banerjee, A., "Dynamics and Control of the WISP Shuttle-Antennae System," *Journal of the Astronautical Sciences*, Vol. 41, No. 1, 1993, pp. 73–90.

[9] Banerjee, A., Pedreiro, N., and Singhose, W., "Vibration Reduction for Flexible Spacecraft Following Momentum Dumping with/Without Slewing," *Journal of Guidance, Control, and Dynamics*, Vol. 24, May–June 2001, pp. 417–428. doi:10.2514/2.4737

[10] Gorinevsky, D., and Vukovich, G., "Nonlinear Input Shaping Control of Flexible Spacecraft Reorientation Maneuver," *Journal of Guidance, Control, and Dynamics*, Vol. 21, No. 2, 1998, pp. 264–270. doi:10.2514/2.4252

[11] Hu, Q., "Input Shaping and Variable Structure Control for Simultaneous Precision Positioning and Vibration Reduction of Flexible Spacecraft with Saturation Compensation," *Journal of Sound and Vibration*, Vol. 318, Nos. 1–2, 2008, pp. 18–35. doi:10.1016/j.jsv.2008.03.068

[12] Parman, S., and Koguchi, H., "Rest-to-Rest Attitude Maneuvers and Residual Vibration Reduction of a Finite Element Model of Flexible Satellite by Using Input Shaper," *Shock and Vibration*, Vol. 6, 1999, pp. 11–27.

[13] Singhose, W., Bohlke, K., and Seering, W., "Fuel-Efficient Pulse Command Profiles for Flexible Spacecraft," *Journal of Guidance, Control, and Dynamics*, Vol. 19, No. 4, 1996, pp. 954–960. doi:10.2514/3.21724

[14] Singhose, W., Derezinski, S., and Singer, N., "Extra-Insensitive Input Shapers for Controlling Flexible Spacecraft," *Journal of Guidance, Control, and Dynamics*, Vol. 19, No. 2, 1996, pp. 385–91.

[15] Singhose, W., Biediger, E., Okada, H., and Matunaga, S., "Closed-Form Specified-Fuel Commands for On-Off Thrusters," *Journal of Guidance, Control, and Dynamics*, Vol. 29, 2006, pp. 606–11. doi:10.2514/1.21932

[16] Singhose, W. E., Porter, L. J., Tuttle, T. D., and Singer, N. C., "Vibration Reduction Using Multi-Hump Input Shapers," *Journal of Dynamic Systems, Measurement, and Control*, Vol. 119, June 1997, pp. 320–326. doi:10.1115/1.2801257

[17] Tuttle, T., and Seering, W., "Experimental Verification of Vibration Reduction in Flexible Spacecraft Using Input Shaping," *Journal of Guidance, Control, and Dynamics*, Vol. 20, No. 4, 1997, pp. 658–664. doi:10.2514/2.4128

[18] Liu, Q., and Wie, B., "Robust Time-Optimal Control of Uncertain Flexible Spacecraft," *Journal of Guidance, Control, and Dynamics*, Vol. 15, No. 3, 1992, pp. 597–604. doi:10.2514/3.20880

[19] Singh, T., and Vadali, S. R., "Robust Time-Optimal Control: A Frequency Domain Approach," *Journal of Guidance, Control, and Dynamics*, Vol. 17, 1994, pp. 346–353. doi:10.2514/3.21204

[20] Singer, N., and Seering, W., "Preshaping Command Inputs to Reduce System Vibration," *Journal of Dynamic Systems, Measurement, and Control*, Vol. 112, March 1990, pp. 76–82. doi:10.1115/1.2894142

[21] Hyde, J., and Seering, W., "Using Input Command Pre-Shaping to Suppress Multiple Mode Vibration," *IEEE International. Conference on Robotics and Automation*, Inst. of Electronic and Electrical Engineers, Piscataway, NJ, 1991, pp. 2604–2609.

[22] Kim, D., and Singhose, W., "Performance Studies of Human Operators Driving Double-Pendulum Bridge Cranes," *Control Engineering Practice*, Vol. 18, 2010, pp. 567–576. doi:10.1016/j.conengprac.2010.01.011

[23] Singhose, W., Crain, E., and Seering, W., "Convolved and Simultaneous Two-Mode Input Shapers," *IEE Control Theory and Applications*, Vol. 144, Nov. 1997, pp. 515–520. doi:10.1049/ip-cta:19971439

[24] Singhose, W., Kim, D., and Kenison, M., "Input Shaping Control of Double-Pendulum Bridge Crane Oscillations," *Journal of Dynamic Systems, Measurement, and Control*, Vol. 130, May 2008, Paper 034504. doi:10.1115/1.2907363

[25] Eloundou, R., and Singhose, W., "Justification for Using Step-Function Reference Commands: Comparison to S-Curves," *2nd IFAC Conference on Mechatronic Systems*, Berkeley, CA, 2002.

[26] Liu, K.-P., and Li, Y.-C., "Vibration Suppression for a Class of Flexible Manipulator Control with Input Shaping Technique," *Fifth International Conference on Machine Learning and Cybernetics*, 2006, pp. 835–839.

[27] Farrenkopf, R. L., "Optimal Open-Loop Maneuver Profiles for Flexible Spacecraft," *Journal of Guidance and Control*, Vol. 2, 1979, pp. 491–498. doi:10.2514/3.55914

[28] Meckl, P. H., Arestides, P. B., and Woods, M. C., "Optimized S-Curve Motion Profiles for Minimum Residual Vibration," *American Control Conference*, Philadelphia, 1998.

[29] Meckl, P., and Seering, W., "Experimental Evaluation of Shaped Inputs to Reduce Vibration for a Cartesian Robot," *Journal of Dynamic Systems Measurement and Control*, Vol. 112, June 1990, pp. 159–165. doi:10.1115/1.2896122

[30] Meckl, P. H., and Seering, W. P., "Minimizing Residual Vibration for Point-to-Point Motion," *Journal of Vibration, Acoustics, Stress, and Reliability in Design*, Vol. 107, Oct. 1985, pp. 378–382.

[31] Meckl, P. H., and Seering, W. P., "Reducing Residual Vibration in Systems with Time Varying Resonances," *IEEE International Conference on Robotics and Automation*, Inst. of Electronic and Electrical Engineers, Piscataway, NJ, 1987, pp. 1690–1695.

[32] Swigert, C. J., "Shaped Torque Techniques," *Journal of Guidance and Control*, Vol. 3, No. 5, 1980, pp. 460–467. doi:10.2514/3.56021

[33] Wiederrich, J. L., and Roth, B., "Dynamic Synthesis of Cams Using Finite Trigonometric Series," *Journal of Engineering for Industry*, Vol. 97, Ser. B, Feb. 1975, pp. 287–293.

[34] Sudarshan, P. B., and Miu, D. K., "Precise Point-to-Point Positioning Control of Flexible Structures," *Journal of Dynamic Systems, Measurement, and Control*, Vol. 112, No. 4, 1990, pp. 667–674. doi:10.1115/1.2896193

[35] Singhose, W., Singer, N., and Seering, W., "Time-Optimal Negative Input Shapers," *Journal of Dynamic Systems, Measurement, and Control*, Vol. 119, June 1997, pp. 198–205. doi:10.1115/1.2801233

[36] Pao, L. Y., and Singhose, W. E., "Verifying Robust Time-Optimal Commands for Multi-Mode Flexible Spacecraft," *Journal of Guidance, Control, and Dynamics*, Vol. 20, No. 4, 1997, pp. 831–833. doi:10.2514/2.4123

[37] Singh, T., and Vadali, S. R., "Robust Time-Delay Control," *Journal of Dynamic Systems, Measurement, and Control*, Vol. 115, 1993, pp. 303–6.

[38] Singh, T., and Heppler, G. R., "Shaped Input Control of a System with Multiple Modes," *Journal of Dynamic Systems, Measurement, and Control*, Vol. 115, Sept. 1993, pp. 341–347.

[39] Grosser, K., Fortgang, J., and Singhose, W., "Limiting High Mode Vibration and Rise Time in Flexible Telerobotic Arms," *Conference on Systemics, Cybernetics, and Informatics*, Orlando, FL, 2000.

[40] Singer, N., and Seering, W., "An Extension Of Command Shaping Methods for Controlling Residual Vibration Using Frequency Sampling," *IEEE International Conference on Robotics and Automation*, Vol. 1, Inst. of Electronic and Electrical Engineers, Piscataway, NJ, 1992, pp. 800–805.

[41] Singhose, W., Seering, W., and Singer, N., "Input Shaping For Vibration Reduction with Specified Insensitivity to Modeling Errors," *Japan-USA Symposium on Flexible Automation*, Boston, MA, 1996.

[42] Singhose, W., Seering, W., and Singer, N., "Residual Vibration Reduction Using Vector Diagrams to Generate Shaped Inputs," *Journal of Mechanical Design*, Vol. 116, June 1994, pp. 654–659. doi:10.1115/1.2919428

[43] Lawrence, J., Singhose, W., Weiss, R., and Erb, A., and Glauser, U., "An Internet-Driven Tower Crane for Dynamics and Controls Education," *IFAC Symposium on Control Education*, Madrid, 2006.